

This is the author's peer reviewed, accepted manuscript. However, the online version of record will be different from this version once it has been copyedited and typeset.

PLEASE CITE THIS ARTICLE AS DOI: 10.1063/5.0227594

AIP/123-QED

Engineering magnetic chirality in FeGe nanocylinders: Exploring topological states for spintronic applications

Eduardo Saavedra,¹ Lucy A. Valdez*,^{2,3} Pablo Díaz,⁴ Noelia Bajales,^{5,6} and Juan Escribá,^{1,7}

¹*Departamento de Física, Universidad de Santiago de Chile (USACH), Santiago, Chile.*

²*Facultad de Ciencias Exactas y Naturales y Agrimensura (FaCENA), Universidad Nacional del Nordeste (UNNE), Corrientes, Argentina.*

³*Instituto de Modelado e Innovación Tecnológica (IMIT), CONICET, Corrientes, Argentina.*

⁴*Departamento de Ciencias Físicas, Universidad de La Frontera (UFRO), Temuco, Chile.*

⁵*Instituto de Física Enrique Gaviola (IFEG), CONICET, Córdoba, Argentina.*

⁶*Facultad de Matemática, Astronomía, Física y Computación (FAMAF), Universidad Nacional de Córdoba (UNC), Córdoba, Argentina.*

⁷*Center for the Development of Nanoscience and Nanotechnology (CEDENNA), Santiago, Chile.*

(*Electronic mail: lvaldez@unne.edu.ar)

(Dated: 23 November 2024)

This is the author's peer reviewed, accepted manuscript. However, the online version of record will be different from this version once it has been copyedited and typeset.

PLEASE CITE THIS ARTICLE AS DOI: 10.1063/1.50227594

Iron germanide (FeGe) emerges as a promising magnetic alloy for spintronics and high-density data storage, owing to its distinctive magnetic properties and compatibility with existing fabrication techniques. This compatibility enables the synthesis of customized FeGe nanocylinders characterized by chirality, where their magnetization asymmetrically twists. Within specific size parameters, these nanocylinders can accommodate skyrmions - swirling magnetic structures with significant implications for information storage and processing technologies. This study investigates the response of FeGe nanocylinders to external magnetic fields, focusing on how their magnetic properties vary with dimensions (diameter and length). Specifically, we analyze the impact of length on the pseudo-static properties of short FeGe nanocylinders and examine the average topological charge and remanence states across different aspect ratios. Our investigation underscores the relationship between chirality and diverse magnetization states in four types of nanocylinders with varying aspect ratios. This comprehensive analysis elucidates the connection between nanocylinder magnetic states and the average topological charge - a critical factor in advancing ultra-low-energy data storage and logic devices.

This is the author's peer reviewed, accepted manuscript. However, the online version of record will be different from this version once it has been copyedited and typeset.

PLEASE CITE THIS ARTICLE AS DOI: 10.1063/1.5027594

Magnetic skyrmions are swirling, chiral nanostructures with vortex-like spin textures, often referred to as chiral magnetic skyrmions (CMSs)^{1–3}. Characterized by their topological stability at the nanoscale, these formations result from the interplay between strong spin-orbit coupling and the broken inversion symmetry of the crystal lattice in ferromagnets that exhibit Dzyaloshinskii-Moriya interaction (DMI) under an external magnetic field^{4–8}. Skyrmions have gained significant attention in recent years due to their potential applications in future spintronic devices. These non-collinear, stable magnetic textures are characterized by a topological charge and exhibit geometric properties such as polarity, helicity, and vorticity. These topological characteristics can be understood through a stereographic projection, making them topologically non-trivial magnetic objects in two-dimensions^{9–11}.

The field of nanomaterials has seen a significant surge in interest in exploring the properties of chiral magnetic textures in nanostructures. This interest is driven by their high potential for applications in spintronics, magnetic data storage, and biomedical sensing^{12–14}. Recently, the focus has expanded beyond nanowires (MNWs) to include a wider range of geometries, such as nanocylinders and nanodots. Recent breakthroughs have shown that manipulating the diameter of these nanostructures can significantly influence the magnetic configurations they can support^{15–22}. These diverse nanostructures offer promising prospects for hosting and manipulating skyrmions. This ability to engineer complex magnetic landscapes within these nanostructures opens doors to a diverse range of stable and controllable magnetic states for CMSs. Such versatile magnetic textures offer exciting possibilities for applications requiring multi-state storage or logic elements, such as high-density magnetic memories, racetrack memories, or non-Boolean logic devices^{7,8,12,23}.

Among the materials that show DMI, iron germanide (FeGe), a non-centrosymmetric cubic helimagnet (space group $P2_13$, B20-type structure), is one of those that stands out^{24–27}. This material can be formed at atmospheric pressure and shows skyrmions close to room temperature^{28,29}, making it an excellent prototype for studying nanostructure chiral properties. The key to its suitability lies in its intrinsic chirality exhibited through asymmetric magnetization at the nanoscale. Moreover, in this material, the skyrmions have an approximate diameter of 70 nm²⁸, a size that allows them to be confined within nanocylinders with diameters of around 100 nm. This makes FeGe an ideal candidate for hosting skyrmions with distinctive characteristics that can emerge under specific size-dependent conditions within tailored nanostructures^{15,30,31}. However, despite extensive theoretical investigations, a complete understanding of the intricate relationship between

chirality and the magnetic states of FeGe in cylindrical nanostructures with diameters between 50 and 200 nm and lengths between 25 and 200 nm remains elusive. Clarifying this connection would provide deeper insights into micromagnetic behavior and offer a critical perspective on the design advantages and limitations of electronic devices utilizing skyrmionic FeGe systems.

This work investigates the size-dependent magnetic properties of FeGe nanocylinders under an external magnetic field applied along the z -axis. Our aim is to unravel the interplay between geometrical parameters and magnetic behavior. We will study how coercivity and remanence vary with changes in the diameter and length of these nanocylinders. Additionally, we will identify magnetization states and their link to chirality, employing various nanostructures with varying aspect ratios. This in-depth exploration aims to elucidate the relationship between their magnetic states and the average topological charge, a crucial property for data storage and logic devices with ultra-low energy consumption.

The quasi-static magnetic properties of FeGe magnetic nanocylinders were studied using the open-source software Mumax³², which solves the Landau-Lifshitz-Gilbert equation using the finite difference method. The equation is expressed as follows

$$\frac{d\mathbf{M}}{dt} = -\gamma (\mathbf{M} \times \mathbf{H}_{\text{eff}}) + \frac{\alpha}{M_s} \left(\mathbf{M} \times \frac{d\mathbf{M}}{dt} \right) \quad (1)$$

where γ denotes the gyromagnetic ratio of the free electron spin and α represents a phenomenological damping constant. This equation describes both the precession and relaxation motions of the magnetization \mathbf{M} under the influence of an effective field \mathbf{H}_{eff} .

Short magnetic nanocylinders were simulated with varying diameters (D) and lengths (L). In this study, we varied the length (L) from 50 nm to 200 nm in steps of 25 nm, while the diameter (D) was chosen from four values ranging from 50 nm to 200 nm, each 50 nm apart. These dimensions were selected based on their experimental feasibility and the intriguing magnetic properties observed in similar investigations³³.

Micromagnetic simulations were conducted with an exchange stiffness constant (A) set to $8.78 \times 10^{-12} \text{ J m}^{-1}$, a saturation magnetization (M_s) of $3.84 \times 10^6 \text{ A m}^{-1}$, and a DMI constant (D_b) of $1.58 \times 10^{-3} \text{ J m}^{-2}$, in line with previous research on FeGe nanomaterials^{30,34-39}. To investigate the pseudo-static magnetic properties, the damping coefficient was set to $\alpha = 0.5$ ^{18,40}. The simulation space was discretized into cells of $2.5 \times 2.5 \times 2.5 \text{ nm}^3$ along the x , y , and z directions, with the z -axis aligned with the main axis of the nanocylinders.

An external magnetic field ($\mu_0\mathbf{H}$) was applied parallel to the nanocylinder axis, with a 1° offset

to break the symmetry condition. The field magnitude was varied from 4000 mT to -4000 mT in steps of 2 mT. A maximum torque condition of $\tau_{\max}/\gamma_0 < 10^{-4}$ T was used to ensure that the magnetization reached equilibrium at each field intensity^{40,41}. Skyrmion stability is described by the topological charge (Q) or by geometric parameters such as polarity (p), helicity (γ), and vorticity (m)⁹⁻¹¹:

$$Q = \frac{1}{4\pi} \int_S \mathbf{m} \cdot \left(\frac{\partial \mathbf{m}}{\partial x} \times \frac{\partial \mathbf{m}}{\partial y} \right) dx dy \quad (2)$$

or in terms of geometric quantities,

$$Q = p \cdot m \quad (3)$$

Polarity ($p = \pm 1$) refers to the magnetization direction at the skyrmion core along the z -axis, while vorticity ($m = 0, \pm 1, \pm 2, \dots$) indicates the sense of in-plane magnetization rotation when tracing magnetic moments in a closed loop around the skyrmion core. Therefore, a skyrmion is defined by a magnetization density that cannot be continuously transformed into a ferromagnetic state without discontinuous changes in the density.

In Fig. 1, normalized hysteresis curves are shown for FeGe nanocylinders with diameters (D) of 50 nm, 100 nm, 150 nm, and 200 nm. These curves were obtained by applying an external magnetic field ranging from 4000 mT to -4000 mT, inclined at 1° from the z -axis (all curves were plotted in a lower range of the applied field for ease of viewing). Hysteresis loops with similar shapes are observed for the cases with diameters of 100 nm, 150 nm, and 200 nm. It is interesting to note that these curves show several points that do not follow a monotonic behavior, such as $D = 200$ nm, $L = 50$ nm, and a field of approximately 300 mT. These abrupt changes are primarily due to a modification in the magnetic texture that minimizes the torque in the nanocylinder. In the mentioned example, this involves a transition from a S-type state to a target skyrmion (see Fig. S1 in the Supplementary Material). In contrast, the behavior for $D = 50$ nm is markedly different, with noticeably higher coercivity and remanence compared to the other diameters. Furthermore, a notable decrease in coercivity is observed as the diameter increases, except for the nanostructures with 50 nm diameter, where coercivity shows a non-monotonic behavior with increasing L (which will be discussed below).

To facilitate a comparative analysis between geometric parameters (diameter and length) and magnetic properties (coercivity and remanence), Fig. 2 illustrates these properties as a function of length. Fig.2(a) shows that coercivity exhibits a non-monotonic behavior, with a sharp decline

This is the author's peer reviewed, accepted manuscript. However, the online version of record will be different from this version once it has been copyedited and typeset.

PLEASE CITE THIS ARTICLE AS DOI: 10.1063/1.50227594

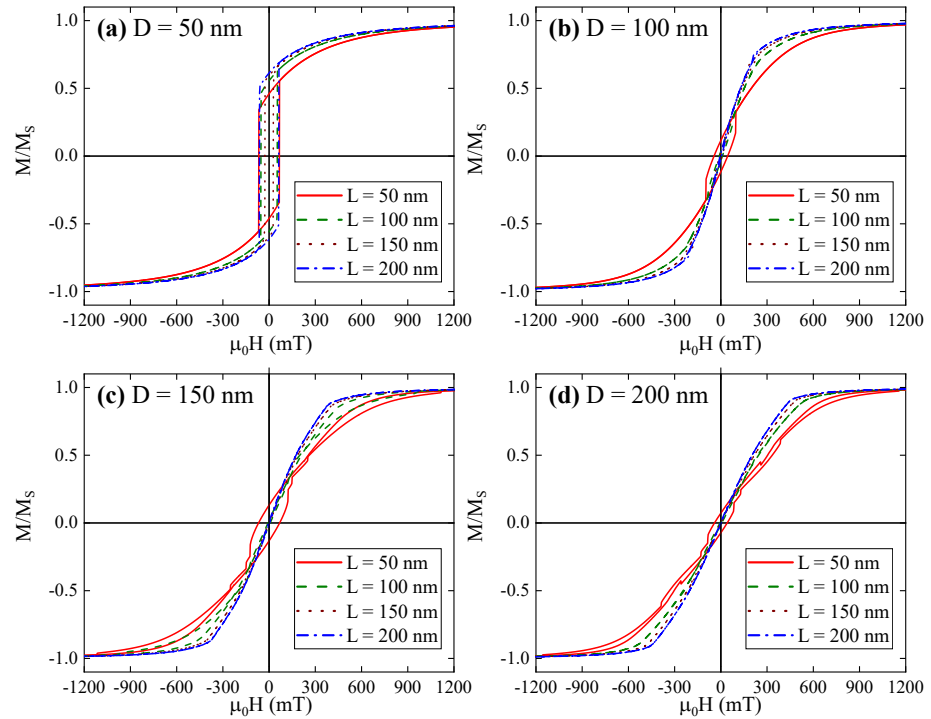


FIG. 1. Normalized simulated magnetic hysteresis loops of FeGe nanocylinders with diameters (D) of (a) 50 nm, (b) 100 nm, (c) 150 nm, and (d) 200 nm, when the external magnetic field is applied at an angle of 1° from the z direction.

up to lengths of 100 nm for all cases. For the smallest diameter nanocylinder ($D = 50$ nm), a significant increase in coercivity is observed for lengths greater than 100 nm, with a particular outlier at $L = 100$ nm. This is due to a slight change in the reversal mechanism, as it involves the nucleation and annihilation of a skyrmionic structure while bypassing the helical state (see Fig. S1 in Supplementary Material). In contrast, coercivity remains near zero for the other analyzed diameters. Fig. 2(b) illustrates that for $D = 50$ nm, remanence increases monotonically with increasing length, reaching its highest value of $0.6 M_r/M_s$ for $L = 200$ nm. In contrast, remanence shows a slight decrease for other diameters, with no significant discrepancies observed between their values. For longer lengths, remanence remains nearly constant and close to zero.

To better understand the topologically non-trivial nature of the magnetic configurations, we

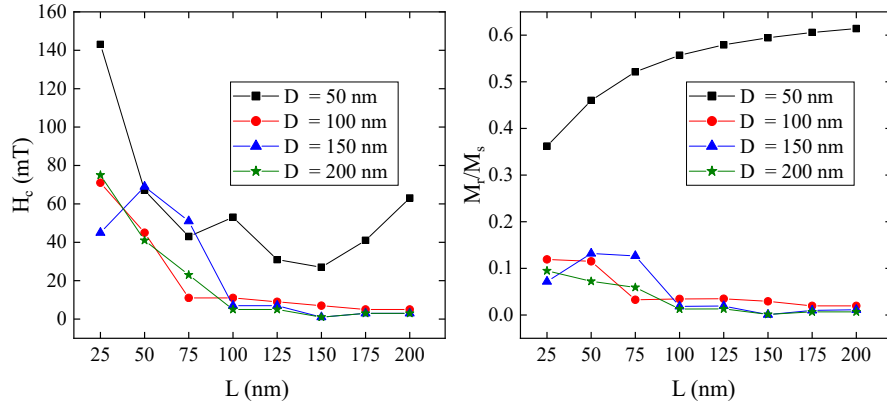


FIG. 2. (a) Coercivity and (b) normalized remanence for FeGe nanocylinders as a function of the length L , when the external magnetic field is applied at an angle of 1° from the z direction.

calculated the value of the 2D topological charge for various cross-sections across the short-length nanocylinders using the following equation:

$$Q = \frac{1}{4\pi} \int_S \mathbf{m} \cdot \left(\frac{\partial \mathbf{m}}{\partial x} \times \frac{\partial \mathbf{m}}{\partial y} \right) dx dy \quad (4)$$

Although the concept of the topological charge (skyrmion number or degree of mapping) in 2D spin systems is not directly applicable to these short nanocylinders due to the dependence of magnetization on the z coordinate, $m(x, y, z)$, several studies report 2D topological charge analysis as a function of the z coordinate^{42–44}.

In Fig. 3, we illustrate the magnetization states in FeGe nanocylinders for sixteen distinct geometric configurations (the same as in Fig. 1) in the absence of an external magnetic field ($\mu_0 \mathbf{H} = 0$). For each configuration, we present the corresponding average magnetic charge $\langle Q \rangle = \sum_{i=1}^N Q_i / N$, where N is the number of cross-sections ($N = L / \Delta z$, with $\Delta z = 2.5$ nm).

We begin our discussion with the case $D = 50$ nm, where the magnetic states are associated with incomplete skyrmions or quasi-ferromagnetic states, indicating no full spin rotation along the diameter. The average topological charge $\langle Q \rangle$ is approximately 0.4 for all four lengths of the nanocylinders. The consistency of $\langle Q \rangle$ across all lengths suggests that the chiral structure remains almost unchanged for each cross-section, regardless of the nanocylinder's length.

This is the author's peer reviewed, accepted manuscript. However, the online version of record will be different from this version once it has been copyedited and typeset.
 PLEASE CITE THIS ARTICLE AS DOI: 10.1063/1.50227594

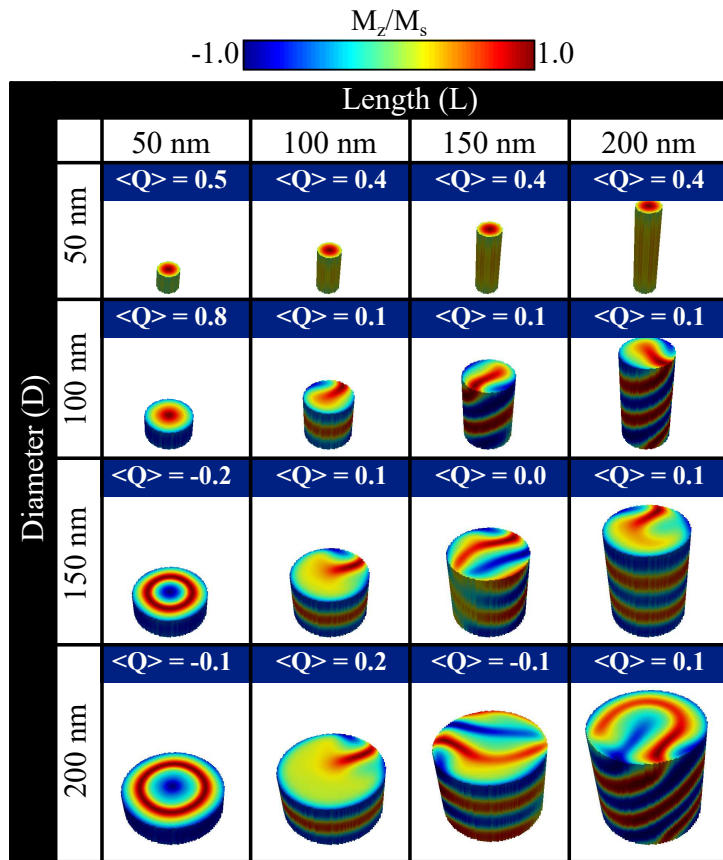


FIG. 3. (a) Magnetization states of sixteen FeGe nanostructures at zero external magnetic field ($\mu_0\mathbf{H} = 0$). The 3D plots show the z component of the magnetization accompanied by the magnitude of the average topological charge $\langle Q \rangle$.

For the case $D = 100$ nm, a significant change is observed between $L = 50$ nm and longer lengths. At the shortest length, a 2π skyrmion with $\langle Q \rangle = 0.8$ is present, while at longer lengths, a mix of U and helix states emerges with $\langle Q \rangle = 0.1$. Again, the chiral structure remains consistent across cross-sections. In the cases of $D = 150$ nm and 200 nm, a target state with two full spin rotations along the diameter and a negative value of $\langle Q \rangle$ is observed at the shortest length. However, as the length increases, mixed and S states are observed, and the value of $\langle Q \rangle$

becomes positive, except for ($D = 200$ nm, $L = 150$ nm).

Considering the length (L), as the diameter increases, skyrmion systems are observed for 50 nm, U states for 100 nm, and mixed or S-states for 150 and 200 nm. Some of these magnetic states were also found in other FeGe nanostructures with similar aspect ratios^{15,35,45}. Notably, skyrmion-type systems were found for $L = 50$ nm nanocylinders regardless of the considered diameters.

With the aim of delving deeper into the emergence of these magnetic textures, variations in demagnetization, exchange, and Dzyaloshinskii-Moriya interaction (DMI) energy densities were examined as a function of nanocylinder lengths for diameters of 50, 100, and 200 nm (Supplementary Figs. S6, S7, and S8). A general trend of decreasing demagnetization energy density with increasing length L was observed. Nanocylinders with $D = 50$ nm exhibited higher demagnetization energy density compared to those with $D = 200$ nm for all lengths L , suggesting that thinner nanocylinders are more prone to demagnetization, while thicker ones are more magnetically stable. Unlike demagnetization energy density, exchange energy density tended to increase with increasing length L for diameters of 100 and 200 nm. This indicates that as the cylinder becomes longer, the energy associated with the magnetic ordering of spins also increases. The dependence of DMI energy on length L and diameter D showed non-monotonic behavior with local maxima and minima, suggesting that DMI is highly sensitive to the geometric dimensions of the system. While for a length of 50 nm, the energy densities of the larger diameter nanocylinders differed from that of the smaller diameter nanocylinder, a trend towards a certain value was observed as the length increased. Correlating these energies with the topological charge values from Fig. 3, it is observed that the formation of skyrmionic systems at zero field is more probable when the FeGe nanocylinder resembles disk-like systems with a negative chiral charge. For aspect ratios of the order of unity or greater with positive chiral charge, the formation of helical states is more likely. A detailed dynamic study is required to determine the sense of clockwise or anticlockwise rotation of these magnetic textures. Such a study would reveal whether both senses are energetically favourable and equally probable, although this is beyond the scope of the present work.

To establish a correlation between the 2D topological charge $\langle Q \rangle$ across various cross-sections along the length of the short nanocylinders and the reversal modes, we analyzed four FeGe nanostructures to depict the hysteresis curve. Our findings are illustrated in Fig. 4. The first case corresponds to a nanodisk with $D = 150$ nm and $L = 50$ nm, i.e., an aspect ratio $L/D = 0.33$. The hysteresis curve shows the existence of a coercive field and remanent magnetization, with a

This is the author's peer reviewed, accepted manuscript. However, the online version of record will be different from this version once it has been copyedited and typeset.

PLEASE CITE THIS ARTICLE AS DOI: 10.1063/1.50227594

central hysteresis area around 0 mT larger than the two other areas located around -600 mT and 600 mT, respectively.

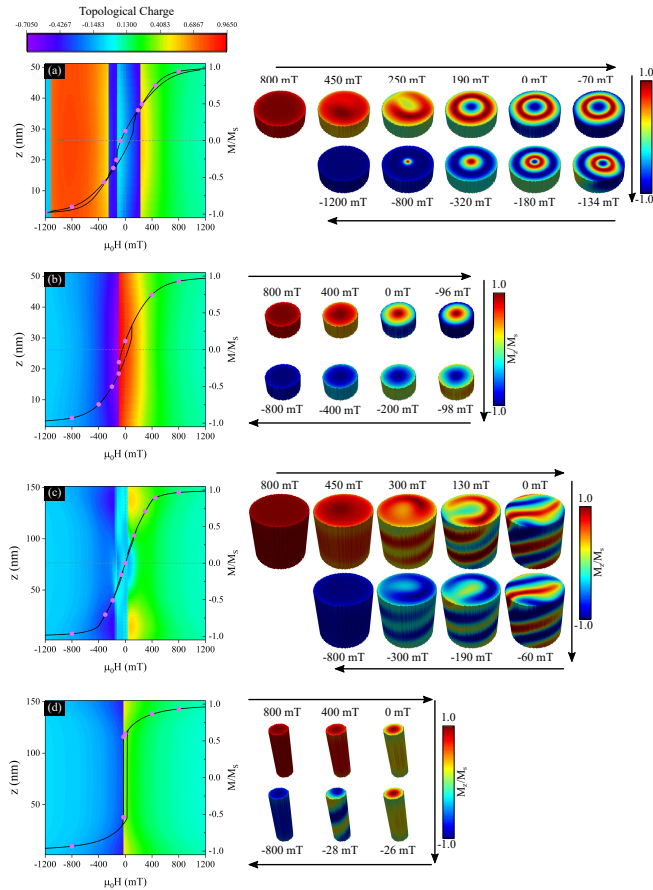


FIG. 4. Hysteresis loops of four FeGe nanostructures alongside a color map of 2D topological charge across various cross-sections along the length of the nanowires. The aspect ratios are 0.33, 0.5, 1.0 and 3.0 for (a), (b), (c), and (d) figures, respectively. Representative points show their magnetization states. The reversal mechanism is displayed in the right panel using a 3D plot of the z component of the magnetization.

At 1200 mT, the magnetic state is uniform, and the 2D topological charge across various cross-sections along the length is $\langle Q \rangle = 0$, indicating behavior typical of a ferromagnetic system. As the applied field decreases, the 2D topological charge $\langle Q \rangle$ becomes positive around 400 mT

and changes to a negative value at 200 mT. The observed magnetic states correspond to target magnetic states for the formation of skyrmionic systems. At 190 mT, an isolated skyrmion (2D topological charge $\langle Q \rangle \approx -0.7$) is observed, followed by target states and a non-rotationally symmetric system at -134 mT (2D topological charge $\langle Q \rangle \approx -0.03$). Target states followed by isolated skyrmion states (2D topological charge $\langle Q \rangle \approx -0.7$) appear around -180 mT, and finally, transitory states are found before a uniform magnetic state is obtained, with a 2D topological charge $\langle Q \rangle \approx 0$. These types of states were also found by Beg et al.⁴⁵ and Carey et al.³⁵ in studies of the reversion mechanism in FeGe nanodisks.

The second case corresponds to a nanocylinder with $D = 100$ nm and $L = 50$ nm, i.e., an aspect ratio $L/D = 0.5$. The hysteresis curve shows the presence of coercive field and remanent magnetization. However, unlike the first case, only a single hysteresis area is observed in the central part around 0 mT. The magnetization reversal is similar to the first situation, but here neither non-rotational symmetry nor U-states are observed. The values of the topological charge changes are different compared to the first situation: at 800 mT, the 2D topological charge $\langle Q \rangle \approx 0.96$, followed by $\langle Q \rangle \approx 0.3$ around 200 mT, $\langle Q \rangle \approx 0.96$ at 0 mT, $\langle Q \rangle \approx -0.7$ at -200 mT, and it becomes $\langle Q \rangle \approx 0$ at 1200 mT.

The third case corresponds to a nanocylinder with $D = 150$ nm and $L = 150$ nm, i.e., an aspect ratio $L/D = 1.0$. The hysteresis curve shows the absence of both coercive field and hysteresis areas, but remanent magnetization is observed. At 1200 mT, it begins with a ferromagnetic state (2D topological charge $\langle Q \rangle = 0$), followed by transitory states until it reaches a U-state at 130 mT (2D topological charge $\langle Q \rangle = 0.27$). S-states are found between 0 mT and -60 mT (2D topological charge $\langle Q \rangle \approx -0.03$), which convert into another U-state at 190 mT (2D topological charge $\langle Q \rangle \approx -0.37$), and finally, the magnetic state changes to a ferromagnetic one at the final reversion (2D topological charge $\langle Q \rangle \approx 0$). These types of states were found by Savchenko et al.¹⁵ in studies of the reversion mechanism in FeGe nanocylinders with an aspect ratio of 1.2.

The fourth case corresponds to a nanocylinder with $D = 50$ nm and $L = 150$ nm, i.e., an aspect ratio $L/D = 3.0$. The hysteresis curve shows a small coercive field and hysteresis area, with remanent magnetization. It begins with a ferromagnetic state at 1200 mT (2D topological charge $\langle Q \rangle \approx 0$), and as the magnetic field decreases, an incomplete skyrmion at 0 mT (2D topological charge $\langle Q \rangle \approx 0.3$) is observed, followed by a mixed state between a bobber and helix at -28 mT (2D topological charge $\langle Q \rangle \approx -0.7$), and finally reaches another ferromagnetic state (2D topological charge $\langle Q \rangle \approx 0$). The 2D topological charge ($\langle Q \rangle$) is positive for applied positive

magnetic fields and negative for applied negative fields, similar to the $\langle Q \rangle$ obtained in the previous nanocylinder.

The results presented in Fig. 4 highlight the crucial role of aspect ratio in reversal dynamics. As previously discussed, the formation of skyrmions, intermediate states such as U-type, S-type, and ferromagnetic states can be observed in elongated nanocylinders. Supplementary Figs. S9, S10, and S11 provide a detailed analysis of the energy density behavior within the hysteresis curve for the four configurations depicted in Fig. 4. When the applied field diminishes towards zero, both demagnetization and exchange energy densities (including DMI) decrease significantly. This is expected, as self-interactions become dominant, influencing the resulting magnetic textures. Regarding demagnetization energy, the energy density difference between regions of strong and weak magnetic fields (ferromagnetic and low-field states, respectively) becomes more pronounced for systems with lower aspect ratios (disks). This indicates that magnetic textures at low fields deviate further from the ferromagnetic state in disks compared to elongated cylinders (aspect ratio 3), where the observed chiral charge is notably lower, as evident in Fig. 4. Conversely, in the case of exchange energy density, abrupt changes are observed, coinciding with topological charge transitions. For instance, the first case in Fig. 4 (aspect ratio 0.33) exhibits three distinct sign changes in topological charge (approximately at 200, -200, and -1100 mT), each leading to a decrease in exchange energy density. These reductions are likely primarily due to DMI, as they are not observed in purely ferromagnetic systems, such as case 4 (aspect ratio 3), which displays a negligible topological charge and minimal variation in exchange energy density upon topological charge inversion.

We investigated the static magnetic properties of short FeGe magnetic nanocylinders with varying aspect ratios, focusing on diameters from $D = 50$ nm to 200 nm (in 50 nm increments) and lengths from $L = 50$ nm to $L = 200$ nm (in 25 nm increments). An external magnetic field was applied between 4000 mT and -4000 mT at an angle of 1 degree from the z -axis.

For nanocylinders with diameters other than 50 nm, coercivity exhibited a non-monotonic decrease up to lengths of 100 nm, with minimal changes observed for lengths up to 200 nm. However, the 50 nm diameter nanocylinder showed the lowest coercivity at a length of 150 nm, with a value of 30 mT, followed by an increase up to 62 mT. In contrast, the remanence for the smallest diameter increased monotonically with length, reaching $0.6 M_r/M_s$, while for the other diameters, remanence remained nearly constant and close to zero.

Furthermore, we calculated the bidimensional topological charge at different cross-sections

along the nanocylinder lengths to determine the magnetization states in FeGe nanocylinders for various aspect ratios. Evaluating sixteen distinct geometric configurations under a zero external magnetic field, we identified U-states for 100 nm and mixed S-states for 150 and 200 nm diameters.

We also examined four different configurations: two nanodisks with aspect ratios of 0.33 and 0.5, a nanorod with an aspect ratio of 1.0, and a short nanowire with an aspect ratio of 3.0. We compared the magnetization reversal mechanisms for each configuration, identifying ferromagnetic, transitory, S-states, and U-states as the primary states.

Our results highlight that chiral magnetic skyrmions can form in short FeGe nanocylinders with aspect ratios lower than one and bidimensional topological charges near 0.14, with an average 2D value of about 0.1. These findings enhance our understanding of the magnetic properties of FeGe nanocylinders, providing insights into their design and potential applications in information storage and processing. This research offers a pathway toward ultra-high-density, energy-efficient, and scalable memory devices.

SUPPLEMENTARY MATERIAL

In the Supplementary Material, a hysteresis loop is displayed for a FeGe nanocylinder (diameter $D = 200$ nm and a length of $L = 50$ nm) to show the propagation of the magnetic texture. The Demagnetization, Exchange and DMI density energies related to Fig.3 are displayed in Figs. S6, S7, and S8 respectively. The variations of Zeeman, demagnetization and exchange energy densities with the external applied field related to Fig.4 are shown in Figs. S9, S10 and S11, respectively. Furthermore, videos (attached to supplemental information, which supports concepts discussed in this work) display the reversal mechanisms of the FeGe nanocylinders studied for the cases: a) $D = 200$ nm and $L = 50$ nm (see SM2.avi), b) $D = 50$ nm and $L = 75$ nm (see SM3.avi), c) $D = 50$ nm and $L = 100$ nm (see SM4.avi), d) $D = 50$ nm and $L = 125$ nm (see SM5.avi).

ACKNOWLEDGMENTS

The authors acknowledge with gratitude the financial support provided by Fondecyt 1240829, Basal Project AFB220001, Secretaría de Ciencia y Tecnología from Universidad Nacional de Córdoba (SECyT, UNC), and Consejo Nacional de Investigaciones Científicas y Técnicas (CONICET).

This is the author's peer reviewed, accepted manuscript. However, the online version of record will be different from this version once it has been copyedited and typeset.

PLEASE CITE THIS ARTICLE AS DOI: 10.1063/5.0227594

REFERENCES

- ¹O. Boulle, J. Vogel, H. Yang, S. Pizzini, D. de Souza Chaves, A. Locatelli, T. O. Mendes, A. Sala, L. D. Buda-Prejbeanu, O. Klein, M. Belmeguenai, Y. Roussigne, A. Stashkevich, S. M. Cherif, L. Aballe, M. Foerster, M. Chshiev, S. Auffret, I. M. Stephane, and G. Gaudin, “Room-temperature chiral magnetic skyrmions in ultrathin magnetic nanostructures,” *Nat. Nanotechnol.* **11**, 449–454 (2016).
- ²F. N. Rybakov and N. S. Kiselev, “Chiral magnetic skyrmions with arbitrary topological charge,” *Phys. Rev. B* **99**, 064437 (2019).
- ³S. Komineas, C. Melcher, and S. Venakides, “Chiral magnetic skyrmions across length scales,” *New J. Phys.* **25**, 023013 (2023).
- ⁴I. Dzyaloshinsky, “A thermodynamic theory of “weak” ferromagnetism of antiferromagnetics,” *J. Phys. Chem. Solids* **4**, 241–255 (1958).
- ⁵T. Moriya, “Anisotropic superexchange interaction and weak ferromagnetism,” *Phys. Rev.* **120**, 91–98 (1960).
- ⁶A. N. Bogdanov and D. Yablonskii, “Thermodynamically stable “vortices” in magnetically ordered crystals. the mixed state of magnets,” *Zh. Eksp. Teor. Fiz* **95**, 178–182 (1989).
- ⁷F. Zheng, F. N. Rybakov, A. B. Borisov, D. Song, S. Wang, Z. Li, H. Du, N. S. Kiselev, J. Caron, A. Kovács, M. Tian, Y. Zhang, S. Blügel, and R. E. Dunin-Borkowski, “Experimental observation of chiral magnetic bobbars in B20-type FeGe,” *Nat. Nanotechnol.* **13**, 451–455 (2018).
- ⁸F. Zheng, N. S. Kiselev, F. N. Rybakov, L. Yang, W. Shi, S. Blügel, and R. E. Dunin-Borkowski, “Hopfion rings in a cubic chiral magnet,” *Nature* **623**, 718–723 (2023).
- ⁹B. Göbel, I. Mertig, and O. A. Tretiakov, “Beyond skyrmions: Review and perspective of alternative magnetic quasiparticles,” *Physics Reports* **895**, 1–28 (2021).
- ¹⁰J.-V. Kim and J. Mulkers, “On quantifying the topological charge in micromagnetics using a lattice-based approach,” *IOP SciNotes* **1**, 025211 (2020).
- ¹¹I. R. de Assis, I. Mertig, and B. Göbel, “Circular motion of noncollinear spin textures in corbino disks: Dynamics of néel- versus bloch-type skyrmions and skyrmioniums,” *Phys. Rev. B* **110**, 064404 (2024).
- ¹²J. Liu, Z. Zhang, and G. Zhao, *Skyrmions: Topological Structures, Properties, and Applications*, Series in Materials Science and Engineering (CRC Press, 2016).

This is the author's peer reviewed, accepted manuscript. However, the online version of record will be different from this version once it has been copyedited and typeset.

PLEASE CITE THIS ARTICLE AS DOI: 10.1063/5.0227594

- ¹³S. Parkin, X. Jiang, C. Kaiser, A. Panchula, K. Roche, and M. Samant, “Magnetically engineered spintronic sensors and memory,” *Proceedings of the IEEE* **91**, 661–680 (2003).
- ¹⁴J. X. H. Yu and H. Schultheiss, “Magnetic texture based magnonics,” *Phys. Rep.* **905**, 1–59 (2021).
- ¹⁵A. S. Savchenko, F. Zheng, N. S. Kiselev, L. Yang, F. N. Rybakov, S. Blügel, and R. E. Dunin-Borkowski, “Diversity of states in a chiral magnet nanocylinder,” *APL Materials* **10**, 061110 (2022).
- ¹⁶F. Zheng, F. N. Rybakov, N. S. Kiselev, D. Song, A. Kovács, H. Du, S. Blügel, and R. E. Dunin-Borkowski, “Magnetic skyrmion braids,” *Nat. Commun.* **12**, 5316 (2021).
- ¹⁷G. Sáez, E. Cisternas, P. Díaz, E. E. Vogel, J. P. Burr, E. Saavedra, and J. Escrig, “Tuning the coercive field by controlling the magnetization reversal process in permalloy modulated nanowires,” *J. Magn. Magn. Mater.* **512**, 167045 (2020).
- ¹⁸G. Sáez, P. Díaz, E. Cisternas, E. E. Vogel, and J. Escrig, “Information storage in permalloy modulated magnetic nanowires,” *Sci. Rep.* **11**, 20811 (2021).
- ¹⁹G. Sáez, E. Saavedra, N. Vidal-Silva, J. Escrig, and E. E. Vogel, “Dynamic susceptibility of a bloch point singularity confined in a magnetic nanowire,” *Results Phys.* **37**, 105530 (2022).
- ²⁰G. Sáez, P. Díaz, N. Vidal-Silva, J. Escrig, and E. E. Vogel, “Bloch points stabilization by means of diameter modulations in cylindrical nanowires,” *Results Phys.* **39**, 105768 (2022).
- ²¹F. Tejo, N. Vidal-Silva, A. P. Espejo, and J. Escrig, “Angular dependence of the magnetic properties of cylindrical diameter modulated Ni₈₀Fe₂₀ nanowires,” *J. Appl. Phys.* **115**, 17D136 (2014).
- ²²J. d’Albuquerque e Castro, D. Altbir, J. C. Retamal, and P. Vargas, “Scaling approach to the magnetic phase diagram of nanosized systems,” *Phys. Rev. Lett.* **88**, 237202 (2002).
- ²³L. Bo, L. Ji, C. Hu, R. Zhao, Y. Li, J. Zhang, and X. Zhang, “Spin excitation spectrum of a magnetic hopfion,” *Appl. Phys. Lett.* **119**, 212408 (2021).
- ²⁴P. Bak and M. Jensen, “Theory of helical magnetic-structures and phase-transitions in MnSi and FeGe,” *J. Phys. C: Solid State Phys.* **13**, L881–L885 (1980).
- ²⁵X. Z. Yu, N. Kanazawa, Y. Onose, K. Kimoto, W. Z. Zhang, S. Ishiwata, Y. Matsui, and Y. Tokura, “Near room-temperature formation of a skyrmion crystal in thin-films of the helimagnet FeGe,” *Nat. Mater.* **10**, 106–109 (2011).
- ²⁶S. X. Huang and C. L. Chien, “Extended Skyrmion Phase in Epitaxial FeGe(111) Thin Films,” *Phys. Rev. Lett.* **108**, 267201 (2012).

This is the author's peer reviewed, accepted manuscript. However, the online version of record will be different from this version once it has been copyedited and typeset.

PLEASE CITE THIS ARTICLE AS DOI: 10.1063/5.0227594

- ²⁷H. Wilhelm, M. Baenitz, M. Schmidt, C. Naylor, R. Lortz, U. K. Roessler, A. A. Leonov, and A. N. Bogdanov, "Confinement of chiral magnetic modulations in the precursor region of FeGe," *J. Phys.: Condens. Matter* **24**, 294204 (2012).
- ²⁸E. Turgut, M. J. Stolt, S. Jin, and G. D. Fuchs, "Topological spin dynamics in cubic FeGe near room temperature," *J. Appl. Phys.* **122**, 183902 (2017).
- ²⁹S. Grytsiuk, M. Hoffmann, J. P. Hanke, P. Mavropoulos, Y. Mokrousov, G. Bihlmayer, and S. Bluegel, "*Ab initio* analysis of magnetic properties of the prototype B20 chiral magnet FeGe," *Phys. Rev. B* **100**, 214406 (2019).
- ³⁰Y. Liu, N. Cai, X. Yu, and S. Xuan, "Nucleation and stability of skyrmions in three-dimensional chiral nanostructures," *Sci. Rep.* **10**, 21717 (2020).
- ³¹F. Zheng, H. Li, S. Wang, D. Song, C. Jin, W. Wei, A. Kovács, J. Zang, M. Tian, Y. Zhang, H. Du, and R. E. Dunin-Borkowski, "Direct imaging of a zero-field target skyrmion and its polarity switch in a chiral magnetic nanodisk," *Phys. Rev. Lett.* **119**, 197205 (2017).
- ³²A. Vansteenkiste, J. Leliaert, M. Dvornik, M. Helsen, F. Garcia-Sanchez, and B. Van Waeyenberge, "The design and verification of MuMax3," *AIP Advances* **4**, 107133 (2014).
- ³³M. P. Proenca, J. Rial, J. P. Araujo, and C. T. Sousa, "Magnetic reversal modes in cylindrical nanostructures: from disks to wires," *Sci. Rep.* **11**, 10100 (2021).
- ³⁴A. C. Booth, Y. Liu, and J. Zang, "Collective modes of three-dimensional magnetic structures: A study of target skyrmions," *J. Magn. Magn. Mater.* **489**, 165447 (2019).
- ³⁵R. Carey, M. Beg, M. Albert, M.-A. Bisotti, D. Cortés-Ortuño, M. Vousden, W. Wang, O. Hovorka, and H. Fangohr, "Hysteresis of nanocylinders with dzyaloshinskii-moriya interaction," *Appl. Phys. Lett.* **109**, 122401 (2016).
- ³⁶M. Beg, R. A. Pepper, D. Cortés-Ortuño, B. Atie, M.-A. Bisotti, G. Downing, T. Kluyver, O. Hovorka, and H. Fangohr, "Stable and manipulable bloch point," *Sci. Rep.* **9**, 7959 (2019).
- ³⁷S. A. Pathak and R. Hertel, "Three-dimensional chiral magnetization structures in FeGe nanospheres," *Phys. Rev. B* **103**, 104414 (2021).
- ³⁸S. A. Pathak, K. Rahir, S. Holt, M. Lang, and H. Fangohr, "Machine learning based classification of vector field configurations," *AIP Advances* **14**, 025004 (2024).
- ³⁹F. Tejo, R. H. Heredero, O. Chubykalo-Fesenko, and K. Y. Guslienko, "The bloch point 3d topological charge induced by the magnetostatic interaction," *Sci. Rep.* **11**, 21714 (2021).
- ⁴⁰A. Pereira, G. Sáez, E. Saavedra, and J. Escrig, "Tunable magnetic properties of interconnected permalloy nanowire networks," *Nanomaterials* **13**, 13 (2023).

This is the author's peer reviewed, accepted manuscript. However, the online version of record will be different from this version once it has been copyedited and typeset.

PLEASE CITE THIS ARTICLE AS DOI: 10.1063/5.0227594

- ⁴¹J. Fullerton, A. Hierro-Rodriguez, C. Donnelly, D. Sanz-Hernández, L. Skoric, D. A. MacLaren, and A. Fernández-Pacheco, "Controlled evolution of three-dimensional magnetic states in strongly coupled cylindrical nanowire pairs," *Nanotechnology* **34**, 125301 (2023).
- ⁴²E. Berganza, M. Jaafar, J. A. Fernandez-Roldan, M. Goiriena-Goikoetxea, J. Pablo-Navarro, A. García-Arribas, K. Guslienko, C. Magén, J. M. De Teresa, O. Chubykalo-Fesenko, and A. Asenjo, "Half-hedgehog spin textures in sub-100 nm soft magnetic nanodots," *Nanoscale* **12**, 18646–18653 (2020).
- ⁴³M. Charilaou, H.-B. Braun, and J. F. Löffler, "Monopole-induced emergent electric fields in ferromagnetic nanowires," *Phys. Rev. Lett.* **121**, 097202 (2018).
- ⁴⁴R. M. Corona, E. Saavedra, S. Castillo-Sepulveda, J. Escrig, D. Altbir, and V. L. Carvalho-Santos, "Curvature-induced stabilization and field-driven dynamics of magnetic hopfions in toroidal nanorings," *Nanotechnology* **34**, 165702 (2023).
- ⁴⁵M. Beg, R. Carey, W. Wang, D. Cortés-Ortuño, M. Vousden, M.-A. Bisotti, M. Albert, D. Chernyshenko, O. Hovorka, R. L. Stamps, and H. Fangohr, "Ground state search, hysteretic behaviour and reversal mechanism of skyrmionic textures in confined helimagnetic nanostructures," *Sci. Rep.* **5**, 17137 (2015).

DATA AVAILABILITY STATEMENT

The data that support the findings of this study are available from the corresponding author upon reasonable request.